EXPERIMENTAL STUDY ON STATISTICAL CHARACTERISTICS OF THE JET DIFFUSION FIELD

Yasuhiko Sakai, Kenji Uchida, Takehiro Kushida
Department of Mechano-Informatics & Systems,
Nagoya University
Furo-cho, Chikusa-ku, Nagoya 464-8603, Japan
ysakai@mech.nagoya-u.ac.jp, kenji-u@sps.mech.nagoya-u.ac.jp, kushitk@mech.nagoya-u.ac.jp

INTRODUCTION

It is important in engineering to clarify the passive scalar diffusion mechanism in turbulent shear flows in relation to the mixing of various fluids and the diffusion of pollutants. Although there are many reports about the measurements of scalar, for example, the temperature difference (Chevray and Tutu,1979, Venkataramani et al.,1975, Browne et al.,1984, Zhu et al .,1988), the concentration of gas (Panchapakesan and Lumely,1993) and the concentration of dye solution (Okada et al.,2001), there still remain the unclear points on the statistical characteristics of scalar (for example, the departure from the local isotropy and the internal intermittency (Warhaft,2000)). In this study, as the fundamental reseach on the passive scalar diffusion in a turbulent flow, the measurements of the instantaneous value of scalar (concentration) at one point in a liquid phase turbulent jet have been made by using the fiber optic concentration sensor, and the distributions of the various scalar statistics obtained from the recorded data were investigated.

EXPERIMENTAL APPARATUS AND CONDITIONS

In this study, the axisymmetric turbulent jet was adopted as a fundamental turbulent shear flow, and the dye of large Schmidt number, which is called C.I.Direct Blue 86 (Schmidt number $Sc \simeq 3,800$), was chosen as a diffusing matter. Figure 1 shows a water channel used in this study. The test section of this channel has a height of 250 mm and a width of 250 mm and the water level is ajusted to 200 mm. The nozzle exit for the jet of the dye solution is 106 mm under the water surface, and located in the center of a channel. This nozzle's exit diameter D is 2.00 mm and the area of the cross section is 3.142 mm^2. The initial concentration C_J is 3.0 g/l and Reynols number $Re = U_J D/\nu$ is about 11,000. The origin of the coordinate system is located at the nozzle exit, and x is the axial coordinate and r is the radial coordinate (see Fig.1).

The concentration of the diffusing matter was measured by the light absorption method (The concentration detecting method based on the Lambert-Beer's law : Nakamura et al.,1983). A optical fiber probe is shown in Fig.2. As a light source, we chose a laser diode with a standard oscillation wavelength of 670 nm since the light of this wavelength is efficiently absorbed by the present dye whose absorbance spectrum shows the maximum around the wavelength of 665 nm. The optical fiber has the outer diameter 0.25 mm and the core diameter 0.01 mm. In the test section the gap between two optical fibers is about 0.6 mm and the control volume is 4.71×10^{-5} mm^3. Here we should note a relation between the scales of the turbulent field and the space resolution of the probe. As the micro length scales of the turbulent field, there are the Taylor length scale λ and the Kolmogolov length scale η, and they are approximated by the following equations (Friehe et al.,1972).

$$\frac{\lambda}{D} = 0.88 Re^{-1/2} \frac{x}{D} \quad (1)$$

$$\frac{\eta}{D} = (48 Re^3)^{-1/4} \frac{x}{D} \quad (2)$$

At $x/D = 30$, the Taylor length scale λ is 0.50 mm and the Kolmogolov length scale η is 0.03 mm, so that the resolution of the present fiber optic probe is considered to be the same order as the Taylor length scale.

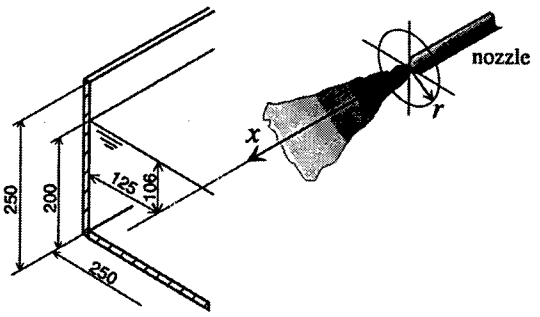

Figure 1: Water channel and coordinate system.

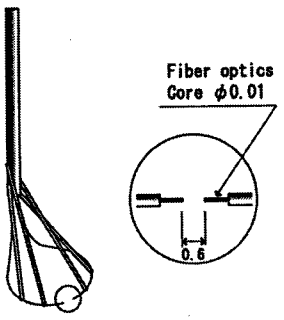

Figure 2: Optical fiber probe.

RESULTS

Fundamental characteristics of the concentration field

The mean concentration. Figure 3 shows the downstream

variation of the mean concentration C along the jet centerline. The abscissa is the downstream distance x normalized by the nozzle exit diameter D and the ordinate is the mean concentration C_C normalized by the initial concentration C_J and its inverce C_J/C_C. From the figure, it is found that C_J/C_C increases linearly in the downstream direction at $x/D \geq 10$ so that the mean concentration is in inverse proportion to downstream distance. The inverse of mean concentration C_J/C_C by the least square approximation is given by

$$\frac{C_J}{C} = 0.190\frac{x}{D} + 0.735. \quad (3)$$

Figure 4 shows the radial profiles of the mean concentration C. The abscissa is the radial distance r normalized by the half width of the mean concentration profile and the ordinate is the mean concentration C normalized by the mean concentration on the centerline C_C. The profile of the mean concentration shows a good similarity in the region of $x/D \geq 30$. Although there is some deviation in the outer region, they are well approximated by the Gaussian curve.

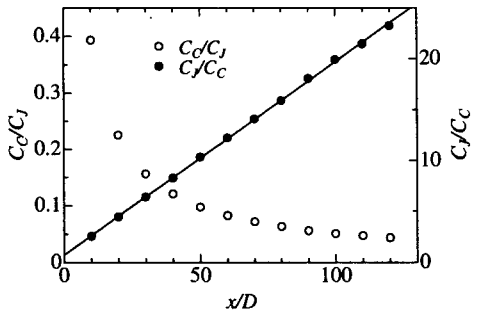

Figure 3: Downstream variation of the mean concentration along the jet centerline.

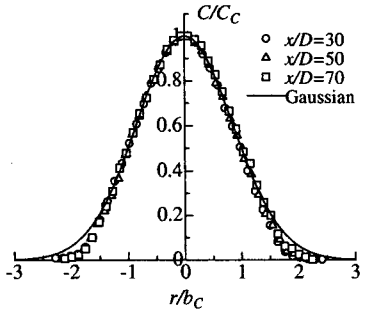

Figure 4: Radial profiles of the mean concentration across the jet.

The concentration fluctuation r.m.s. value. Figure 5 shows the downstream variation of the concentration fluctuation r.m.s. value c'. The ordinate shows the concentration fluctuation c'_C normalized by the initial concentration C_J and its inverce C_J/c'_C. From the figure, we found the concentration fluctuation c'_C is also in inverse proportion to the downstream distance like the mean concentration C_C. The inverse of the concentration fluctuation C_J/c'_C by the least square approximation is given by

$$\frac{C_J}{c'_C} = 0.812\frac{x}{D} + 10.11. \quad (4)$$

Figure 6 shows the radial profiles of the concentration fluctuation r.m.s. value c'. The ordinate is the concentration fluctuation r.m.s. value c' normalized by the value on the centerline c'_C. Although some scattering is observed in the outer region, it shows a good similarity in the region of $x/D \geq 30$, and they have a peak at $r/b_C \simeq 0.9$.

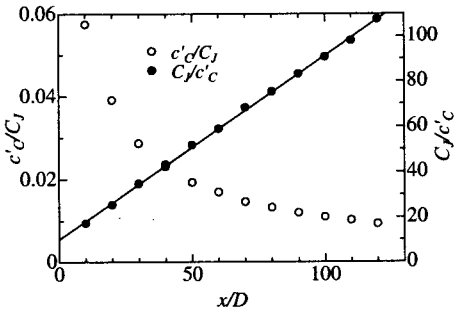

Figure 5: Downstream variation of the concentration fluctuation r.m.s. value along the jet centerline.

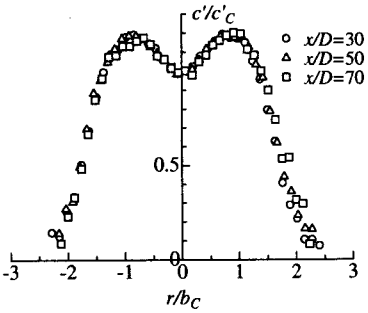

Figure 6: Radial profiles of the concentration fluctuatio r.m.s. value.

Caracteristics of the concentration probability dencity function (p.d.f)

Downstream variation of the concentration p.d.f.. Figure 7 shows the downstream variation of concentration p.d.f. $p(\tilde{c})$, where c is the fluctuation component defined by $c = \tilde{c} - C$ ($\tilde{c}$: concentration instantaneous value), and $p(c)$ and c are normalized by the concentration fluctuation c' respectively. The solid line in the figure represents the Gaussian curve. The distribution of the concentration p.d.f. shows a good similarity in the region of $x/D \geq 30$. However, they deviate from Gaussian distribution and are skewed in the negative side, i.e., they tend to have a long tail in the negative direction.

The skewness and the kurtosis of the concentration p.d.f.. Figure 8 shows the downstream variation of the skewness S and the kurtosis K of the concentration p.d.f. along the jet

centerline. The skewness S and the kurtosis K are respectively difined by

$$S = \int_{-\infty}^{\infty} x'^3 p(x)\,dx \Big/ \left[\int_{-\infty}^{\infty} x'^2 p(x)\,dx\right]^{3/2}, \quad (5)$$

$$K = \left\{\int_{-\infty}^{\infty} x'^4 p(x)\,dx \Big/ \left[\int_{-\infty}^{\infty} x'^2 p(x)\,dx\right]^2\right\} - 3, \quad (6)$$

$x' = x - \mu$, μ : the first order moment of $p(x)$.

When the p.d.f. shows the Gaussian distribution, the skewness S and the kurtosis K are zero. In the present measurements, the skewness S and the kurtosis K have apparantly non-zero values. This is also clear from the distributions of the concentration p.d.f. as shown in Fig.7.

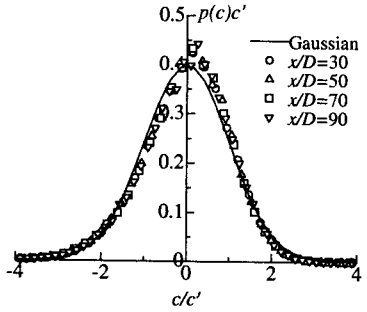

Figure 7: Downstream variation of the concentration p.d.f. along the jet centerline.

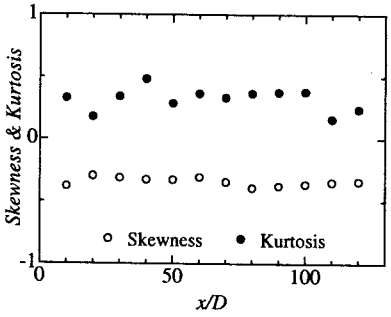

Figure 8: Downstream variation of the skewness and kurtosis of the concentration p.d.f. along the jet centerline.

Orthogonal expansion of the p.d.f.. It is known that the p.d.f. slightly deviated from the Gaussian distribution can be expressed by the Gram-Charlier series (Hino,1977), which is a kind of orthogonal expansions. Here we try to express the concentration p.d.f. by the Gram-Charlier series. The Gram-Charlier expanssion for the concentration p.d.f. $p(\xi)$ is defined by

$$p(\xi) = a_0\phi(\xi) + \frac{a_1}{1!}\phi'(\xi) + \frac{a_2}{2!}\phi''(\xi)\cdots, \quad (7)$$

where ξ is $\xi = (\tilde{c} - C)/c'$, $\phi(\xi)$ is the normal Gaussian p.d.f. and $\phi^{(n)}(\xi)$ is the nth order derivative of $\phi(\xi)$, which is given by

$$\phi^{(n)}(\xi) = (-1)^n H_n(\xi)\phi(\xi). \quad (8)$$

In Eq.(8), $H_n(\xi)$ is the Hermite polynominal and has the orthogonality as follows.

$$\int_{-\infty}^{\infty} H_m(\xi)H_n(\xi)\phi(\xi)\,d\xi = \delta_{mn}(\xi) = \begin{cases} m! & (m = n) \\ 0 & (m \neq n) \end{cases} \quad (9)$$

And the coefficients up to the 6th order of Eq.(7) are defined by

$$a_0 = 1,\ a_1 = a_2 = 0,\ a_3 = -\frac{\mu_3}{c'^3},\ a_4 = \frac{\mu_4}{a'^4} - 3,$$
$$a_5 = -\frac{\mu_5}{c'^5} + 10\frac{\mu_3}{c'^3},\ a_6 = \frac{\mu_6}{c'^6} - 15\frac{\mu_4}{c'^4} + 30, \quad (10)$$

where the nth order moment is defined by

$$\mu_n = \int_{-\infty}^{\infty} \xi^n p(\xi)\,d\xi. \quad (11)$$

Figure 9 shows the concentration p.d.f. obtained by the Gram-Charlier expansion up to 6th order on the jet centerline at $x/D = 50$. From figure, we find the p.d.f. obtained by this orthogonal expansion agrees well with the experimental p.d.f..

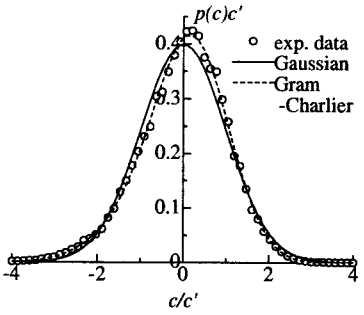

Figure 9: Gram-Charlier expansion of the concentration p.d.f. on the jet centerline at $x/D = 50$.

Random dilution amount model. From the above data analysis, it was found that the concentration p.d.f. on the jet centerline has the skewed distribution. In the plume diffusion field, Csanady (1973) suggested the random dilution model which leads to the log-normal distribution. Here we considered the application of this model to the concentration p.d.f. in the jet diffusion field. Firstly we noticed that the sign of the skewness of the concentration p.d.f. in the jet diffusion field is opposite to the one of the log-normal distribution. Consequently, as a new variable the concentration defect $\hat{c} = C_J - \tilde{c}$ was introduced. Here the fluctuation component of $\hat{c}$ is defined as $\hat{c}_d$ ($\hat{c}_d = \hat{c} - \hat{C}$, $\hat{C}$: the mean of the concentration defect). Then the p.d.f. for $\hat{c}_d$ was calculated and compared with the log-normal distribution. The result was shown in Fig.10. From the figure, it is found that the p.d.f. for $\hat{c}_d$ shows a good agreement with the log-normal distribution. Therefore, in this study, we will suggest a new random dilution model for the concentration defect $\hat{c}$. Since the concentration defect $\hat{c}$ means the dilution amount of matter in the lump of fluid, this model is called the "random dilution amount model" from its physical meaning.

Figure 11 shows the dilution process of the concentration defect by the random dilution amount model. This dilution

process is based on an usual binomial multiplicative process (Feder,1988) and on the line segment the amount of concentration defect $\hat{c} = C_J - \tilde{c}$ is assigned as measure. The dilution amount coefficient β is a random variable which is $\beta \geq 1$ and this is expressed as β_{ij}, $i = 1, 2, \cdots, n$; $j = 1, 2$. It is assumed that β_{ij} has the same probability ditribution regardless of i, j. When an initial amount of concentration defect is $\hat{c}_0 = 1$, the concentration defect in the first cell after n steps is given by

$$\hat{c}_n = C_J - \tilde{c}_n = \beta_{11}\beta_{21} \cdots \beta_{n-1,1}. \quad (12)$$

Moreover, taking the logarithm of both sides, we obtain the following equation,

$$\ln \hat{c}_n = \ln \beta_{11} + \ln \beta_{21} + \cdots \cdots \ln \beta_{n-1,1}. \quad (13)$$

Since $\ln \beta_{11}, \ln \beta_{21}, \cdots, \ln \beta_{n-1,1}$ are random variables which have the same probability characteristics, when n is fully large, by the central limit theorem the probability density for $\hat{c}_n = \zeta$ after n steps is approximated by

$$p_n(\zeta) = \frac{1}{\zeta\sqrt{2\pi}\sigma} \exp\left\{-\frac{(\ln\zeta - \ln\zeta_c)^2}{2\sigma^2}\right\}, \quad (14)$$

where both ζ_c and σ are the functions of n, and given by

$$\ln \zeta_c = nE(\ln \beta_{ij}), \quad (15)$$

$$\sigma = \sqrt{n}\sigma_{ij}, \quad (16)$$

where β_{ij} is the dilution amount coefficient at each step, $E(*)$ is the expectation and σ_{ij} is the standard deviation of $\ln \beta_{ij}$. Since each step is assumed to follow the same probability distribution, $E(\ln \beta_{ij})$ and σ_{ij} are expected to keep constant values independent of i, j. By using Eq.(15) and (16), Eq.(14) is written as

$$p_n(\zeta) = \frac{1}{\zeta\sigma_{ij}\sqrt{2\pi n}} \exp\left\{-\frac{[\ln\zeta - nE(\ln\beta_{ij})]^2}{2(\sigma_{ij}\sqrt{n})^2}\right\}. \quad (17)$$

Hence, we find that the p.d.f. of concentration defect $\hat{c}_n = \zeta_c$ becomes the log-normal distribution.

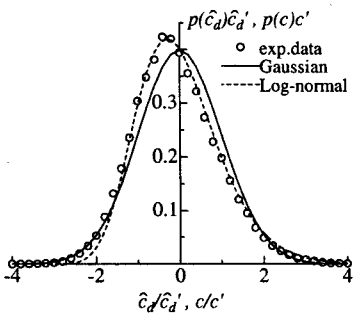

Figure 10: Comparison of the concentration defect p.d.f. with the log-normal distribution at $x/D = 50$.

Radial variation of the concentration p.d.f.. Figure 12 shows the radial variation of the concentration p.d.f. $p(\tilde{c})$ at $x/D = 50$. Although a smooth distribution can be observed around the jet centerline, the large peaks appear at the outer region because of intermittency of the concentration detection/nondetection. It is found that the value of peak became large as the increase of radial distance.

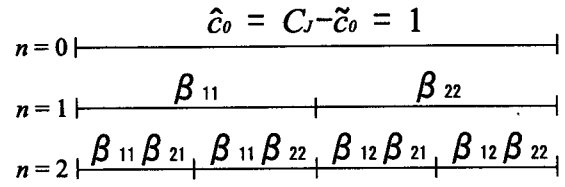

Figure 11: Random dilution amount model on the basis of the binomial multiplicative process.

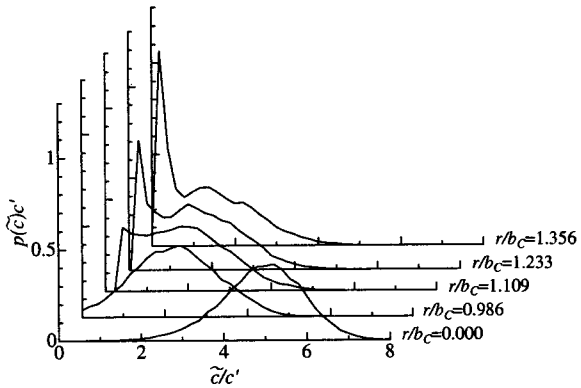

Figure 12: Radial variation of the concentration p.d.f. at $x/D = 50$.

Radial profiles of the intermittency factor

Firstly, we explain about the method to determine the intemittency factor (the Gaussian fitting method, Bilger et al.,1976). For the concentration measurement, the events of detecting and nondetecting the concentration are mutually exclusive. Therefore, the concentration signal can be devided into two regions, i.e., the concentration detecting region and the concentration nondetecting region. Then the ideal p.d.f. $p(\tilde{c})$ is written as follows,

$$p(\tilde{c}) = (1-\gamma)p_f(\tilde{c}) + \gamma p_t(\tilde{c}), \quad (18)$$

where $p_t(\tilde{c})$ is the p.d.f. for the concentration detecting region and $p_f(\tilde{c})$ is the p.d.f. for the concentration nondetecting region. Now, when we define the p.d.f. of the noise signal as $p_n(\tilde{c})$, the acutually measured p.d.f. $p_m(\tilde{c})$ is written by the convolution integral as follows,

$$p_m(\tilde{c}) = \int_{-\infty}^{\infty} p_n(\tilde{c}-\phi)[(1-\gamma)p_f(\tilde{c}) + \gamma p_t(\tilde{c})]\, d\phi. \quad (19)$$

If the p.d.f. for the concentration nondetecting region $p_f(\tilde{c})$ is the delta function $\delta(\tilde{c})$ and the noise signal p.d.f. $p_n(\tilde{c})$ is the Gaussian distribution with standard deviation σ_n, $p_m(\tilde{c})$ is rewritten as

$$p_m(\tilde{c}) = \frac{1-\gamma}{\sigma_n\sqrt{2\pi}} \exp\left[-\frac{\tilde{c}^2}{2\sigma_n^2}\right] + \gamma \int_{-\infty}^{\infty} \frac{1}{\sigma_n\sqrt{2\pi}} \exp\left[-\frac{(\tilde{c}-\phi)^2}{\sigma_n^2}\right] p_t(\phi)\, d\phi \quad (20)$$

The first term on the right hand side in the above equation means the contribution of the nondetecting region, therefore we can get the intermittency factor γ by fitting the Gaussian curve to the p.d.f. distribution around $\tilde{c} = 0$.

Figure 13 shows the radial profiles of the intermittency factor γ obtained by the above method. Here the abscissa is the radial distance r normalized by the half width of the

radial profiles of the intermittency factor b_I. In the figure, the solid line represents the result by Shaughnessy et al (1977). and broken line represents the result by Chevray et al. (1978). It is found that the present slope of decrease of the intermittency factor is larger than the other results.

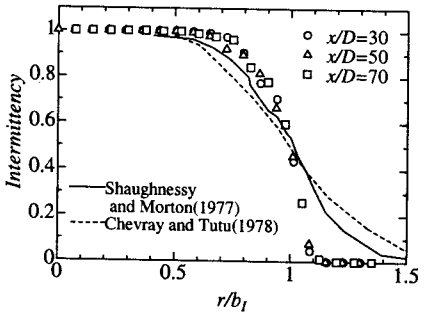

Figure 13: Radial profiles of the intermittency factor.

Radial profiles of the conditional statistics

Threshold level method. To obtain the conditional statistics, It is necessary to determine the threshold value for dividing between the detecting region and the nondetecting region. In this study, the threshold value is determined by comparing the intermittency factor obtained from the intermittency function with the one obtained by the Gaussian fitting method. This method was developed by Nakamura et al. (1999). Here, this method is summarized.

Firstly, the intermittency function is constructed from the discretized concentration signal by giving a threshold value S, as follows,

$$\begin{cases} \tilde{I}_i = 1, & \text{if} \quad \tilde{c}_i \geq S \\ \tilde{I}_i = 0, & \text{if} \quad \tilde{c}_i < S. \end{cases} \tag{21}$$

Then the threshold value is given by

$$S = k\sigma_n, \tag{22}$$

where k is an arbitrary positive real number and σ_n is the standard deviation of the noise signal. k is determined so that the radial profiles of the intermittency factor by the threshold level method will be in agreement with those by the Gaussian fitting method. Figure 14 shows the change of the radial profile of the intermittency factor γ at $x/D = 50$ with the variation of k. Here, the abscissa shows the radial distance r normalized by the half width of the radial profiles of the mean concentration b_C. From the figure it is found that the profile of $k = 5.0$ agrees with the profile obtained by the Gaussian fitting method. Therefore, in this study, $k = 5.0$ is adopted as the threshold value.

Conditional mean concentration. Figure 15 shows the radial profiles of the conditional mean concentration $\langle C \rangle$ with the conventional mean concentration C. The ordinate is the conditional mean concentration $\langle C \rangle$ normalized by the conditional mean concentration on the centerline $\langle C \rangle_C$. As the increase of radial distance, the conditional mean concentration tends to approach to a constant value($\langle C \rangle / \langle C \rangle_C \simeq 0.15$).

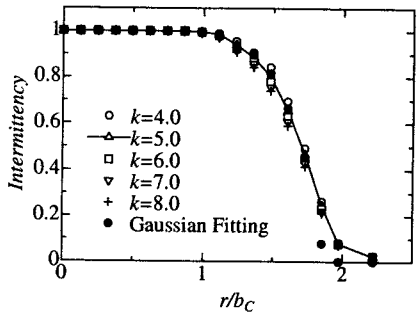

Figure 14: The change of the radial profiles of the intermittency factor by k at $x/D = 50$.

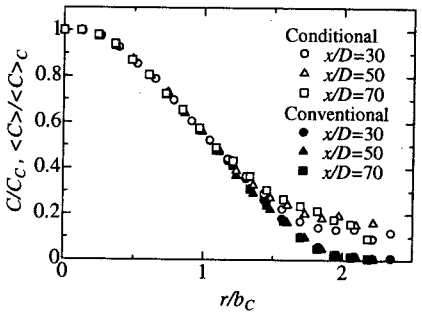

Figure 15: Radial profiles of the conditional and conventional mean concentration.

Conditional concentration fluctuation r.m.s. value. Figure 16 shows the radial profiles of the conditional concentration fluctuation r.m.s. value $\langle c' \rangle$ with the conventional concentration fluctuation r.m.s. value c'. The ordinate shows the conditional concentration fluctuation r.m.s. value $\langle c' \rangle$ normalized by the value on the centerline $\langle c' \rangle_C$. From the figure, it is found that although there is some scattering in the outer region, the conditional concentration fluctuation also tends to approach to a constant value($\langle c' \rangle / \langle c' \rangle_C \simeq 0.4$) as the increase of radial distance.

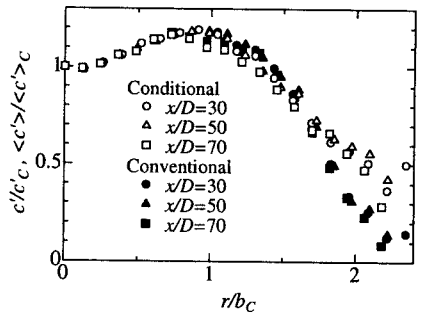

Figure 16: Radial profiles of the conditional and conventional r.m.s. value of the concentration fluctuation.

Conditional concentration p.d.f.. Figure 17 shows the radial variation of the conditional concentration p.d.f. $p^*(\tilde{c})$. In the outer region, the magnitude of peak near $\tilde{c} = 0$ is relatively smaller than the one of conventional concentration p.d.f. $p(\tilde{c})$ (see Fig.12), but the peak still exists. In

the region where the intermittency is high, it is known that the conditional p.d.f. $p^*(\tilde{c})$ becomes an exponential similarity distribution which is given by the following equation (O'brien,1978).

$$p^*(\tilde{c}/\langle C\rangle) = \exp(-\tilde{c}/\langle C\rangle) \tag{23}$$

In this study, the exponential distribution could not be observed since the intermittency is low.

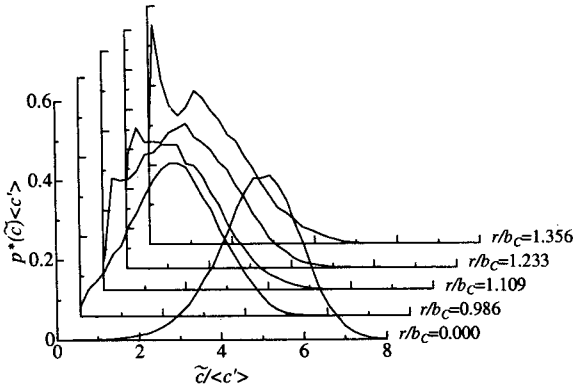

Figure 17: Radial variation of the conditional concentration p.d.f. at $x/D = 50$.

CONCLUSION

1. In the jet diffusion field of the dye solution, the concentration p.d.f. near the jet centerline could be approximated by the Gram-Charlier series expansion. However, to obtain the good approximation of the p.d.f. by the Gram-Charlier series expansion we need the moments of scalar fluctuation up to 6th order or higher. Consequently, it becomes practically very difficult to obtain the concentration p.d.f. from the Gram-Charlier expansion by the numerical simulation. In this study, a new dilution model for the amount of the concentration defect (which is called the "random dilution amount model") was suggested, and it was shown that the p.d.f. for the concentration defect obtained by this model becomes a log-normal distribution, which is in good agreement with the experimental p.d.f. for the concentration defect. Since the log-normal distribution can be determined by the moments up to the second-order, the present random dilution amount model is very effective to predict the concentration p.d.f. by the numerical simulation.

2. The conditional mean concentration $\langle C\rangle$ and the conditional concentration fluctuation r.m.s. value $\langle c'\rangle$ tend to approach to constant values as the increase of radial distance.

REFERENCE

Bilger,R.W., Antonia,R.A. and Sreenivasan,K.R., 1976, "Detemination of intermittency from the probability density function of a passive scalar", *Phys.Fluids*, Vol.19, pp.1471-1475

Browne,L.W.B., Antonia,R.A. and Chambers,A.J., 1984, "The interaction region of a turbulent plane jet", *J.Fluid Mech.*, Vol.149, pp.355-373

Chevray,R. and Tutu,N.K., 1979, "Intermittency and preferential transport of heat in a round jet.", *J.Fluid Mech.*, Vol.88, pp.133-160

Csanady,G., 1973 "Turbulent Diffusion in the Environment", Redial, pp222

Feder,J., 1988, "Fractals", Plenum Press, pp.66-103

Friehe,C.A., Van Atta,C.W. and Gibson,C.H., 1972, "Jet turbulence : dissipation rate measurements and correlations", in *Turbulent Sheer Flows*, AGARD Conference Proceedings, No.93, pp.18.1-18.7

Hino,M. 1977, "Spectral Analysis", Asakura Book Company, pp.115-118, in Japanese

Nakamura,I., Miyata,M. and Sakai,Y., 1983, "On a method of the concentration measurement by the use of light absorption law", *Bulletin of the JSME*, Vol.26, No.218, pp.1357-1365

Nakamura,I., Sakai,Y. and Tsunoda,H., 1999, "On conditional statistics of the diffusion field of matter by a point source plume in conform mean shear flow", *JSME International J.*, Series II, Vol.32, No.2, pp180-188

O'brien,E.E., 1978, "Stochastic properties of scalar quantities advected by a non-buoyant Plume", *J.Fluid Mech.*, Vol.89, Part2, pp.209-222

Okada,Y., Sakai,Y. and Kobayashi,N., 2001, "Structure of the velocity-scalar corelations in an axisymmetric turbulent jet", *Trans. of JSME*, Vol.67, No.664, pp.3085-3092

Panchapakesan,N.R. and Lumely,J.L., 1993, "Turbulence measurements in axisymmetric jets of air and helium, Part2, Helium jet", *J.Fluid mech.*, Vol246, pp.225-247

Shaughnessy,E.J. and Morton,J.B., 1977, "Laser light-scattering measurements of particle concentration in a turbulent jet", Vol.80, part1, pp.129-148

Venkataramani,K.S., Tutu,N.K. and Chevray,P., 1975, "Probability distribution in a round heated jet", *Phys.Fluids*, Vol.18, pp.1413-1420

Warhaft,Z., 2000, "Passive scalars in turbulent flows", *Annu.Rev.Fluid Mech.*, Vol.32, pp.203-240

Zhu,J.Y., So,R.M.C. and Otugen,M.V., 1988, "Turbulent mass flux measurements using a laser/hot-wire technique", *Int.J.Heat Mass Transfer*, Vol.31, pp.819-829